

Chemical deposition of MnO₂ nanosheets on graphene-carbon nanofiber paper as free-standing and flexible electrode for supercapacitors

Yuanzhan Wu¹ · Suqin Liu¹ · Kuangmin Zhao¹ · Zhen He¹ · Hao Yuan¹ · Kezhou Lv¹ · Guofeng Jia¹

Received: 13 November 2015 / Revised: 14 December 2015 / Accepted: 19 December 2015 / Published online: 19 January 2016
© Springer-Verlag Berlin Heidelberg 2016

Abstract Graphene-carbon nanofiber/MnO₂ nanocomposite paper (GMP) is prepared via a simple chemical reaction between KMnO₄ and carbon materials in acidic solution, in which MnO₂ nanosheets are uniformly deposited on the graphene-carbon nanofiber paper. Owing to its freestanding structure, GMP is directly used as an electrode in the electrochemical tests without addition of any binders or conductive additives. Encouragingly, GMP exhibits an excellent capacitive performance with a high specific capacitance of 298.2 F g⁻¹ at 1 A g⁻¹ in 1 M Na₂SO₄ electrolyte. Meanwhile, this composite paper can withstand high scan rate loads without a large decrease of capacitance, the specific capacitance can be remaining at 370.4 F g⁻¹ even at 300 mV s⁻¹. In the cycling test, the composite paper presents an outstanding stability with 95.7 % capacitance retention after 3000 cycles. Additionally, the asymmetric supercapacitor is fabricated based on GMP electrode, it not only shows a high operating voltage of 2.0 V but also exhibits a high energy density of 23.0 Wh kg⁻¹ at 450.8 W kg⁻¹.

Prime novelty statement 1. A simple route to synthesize flexible graphene-carbon nanofiber/MnO₂ nanocomposite paper (GMP).
2. The GMP has free-standing structure to be directly used as electrode without any binders and conductive additives.
3. The GMP electrode exhibits excellent capacitive performance and good cycling life at high current density.
4. GMP-based asymmetric supercapacitor shows a high energy density of 23.0 Wh kg⁻¹ at 450.8 W kg⁻¹.
5. The GMP electrode holds a promising application in flexible supercapacitors.

✉ Suqin Liu
sqliu2003@126.com

¹ College of Chemistry and Chemical Engineering, Central South University, Changsha 410083, China

Therefore, this kind of composite paper would be promising as electrode materials for flexible and high performance supercapacitors.

Keywords Graphene · Carbon nanofiber · Supercapacitor · Manganese dioxide · Composite

Introduction

Supercapacitors, one of the most promising modern energy storage devices, have been widely explored for energy storage applications due to their unique characteristics like high power density, long cycle life (>100,000 cycles), and environmental friendliness [1–3]. Based on the different charge storage mechanisms, supercapacitors are usually categorized as either electrochemical double layer capacitors (EDLCs) or pseudo-capacitors [4]. But as the electrochemical performance of supercapacitors is mainly dependent on their electrodes, the researchers generally pay much more attention to the electrode materials than the electrolyte and membrane. Now, various materials have been investigated to be potential supercapacitors electrode materials. Generally, the carbonaceous materials such as graphene [2, 5, 6], carbon nanofibers (CNFs) [7], and carbon nanotubes (CNTs) [8, 9] are used for EDLCs because of their high surface area, good processing ability, and high conductivity. In contrast, conducting polymers [10, 11] and transition-metal oxides [12, 13] are commonly used for pseudo-capacitors own to their reversible redox reactions in electrolyte. However, noting that the maximum value of the energy and power density in carbon-based double layer capacitors is greatly limited, while conducting polymers and transition-metal oxides have the shortage of poor electronic conductivity [14]. To achieve a high performance supercapacitor, the most accepted strategy is to use

composites of carbonaceous materials, conducting polymers, or transition-metal oxides as its electrode materials [1, 2, 15].

Among the transition-metal oxides, manganese dioxides (MnO_2) have been extensively used as electrode materials for supercapacitors for decades because of their high specific capacitance, abundance, and low toxicity [16, 17]. However, all of the reported specific capacitance values are still far below the theoretical specific capacitance (1370 F g^{-1}) of MnO_2 due to its intrinsic shortage of low electrical conductivity (10^{-5} – $10^{-6} \text{ S cm}^{-1}$) [18]. Supercapacitors based on pure MnO_2 often exhibit poor rate capability and low stability [19–21]. Therefore, to maximize utilization of MnO_2 pseudocapacity, one of the most accepted strategies is to grow nanosized MnO_2 on stable carbon substrates of high electronic conductivity (such as CNTs, CNFs, graphene, etc.) [22–24]. Although these MnO_2 -based composites exhibit an enhanced capacitive performance, but their rate capability still do not show a conspicuous improvement as the addition of binder or conductive additives in preparation of electrodes increases the total electrode weight and the electrode resistance to a degree [25, 26]. Therefore, there is a great significant to develop binder-free electrode materials. Now, various freestanding MnO_2 composite electrodes have been explored using carbon cloth, graphene/carbon nanotube paper, CNTs-embedded CNFs, CNTs paper, and metal foil/foam as the substrate [26–30]. Encouragingly, all these binder-free MnO_2 composites show a greater enhance in specific capacitance, rate capability, and cycling stability compared to the binder-dependent MnO_2 composites.

Graphene, a flat monolayer of hexagonally bonded sp^2 carbon atoms, has been attracted extensive attention in electrochemical energy storage applications owe to its excellent mechanical property, high electronic conductivity, thermal conductivity, elasticity, and specific surface area [2, 31–33]. However, the limits of easy aggregation and restacking between graphene nanosheets have become a serious obstacle for taking the full advantage of graphene [34]. To solve this problem, the usual strategy is to incorporate other nanomaterials into graphene nanosheets [31]. CNFs, another kind of outstanding carbon materials, have also been well-known for not only high mechanical strength but also light, highly conductive, highly porous, bendable [35–40] and can be served as scaffolds in their composites [3]. In recent years, they also have been attractive as excellent electrode materials in various energy storage devices. Therefore, embedding CNFs into graphene nanosheets may allow us to achieve a flexible substrate with light weight, high conductivity, and rough surface; then if depositing nanosized MnO_2 on this kind of substrate, we would obtain a flexible composite paper of high capacitive performance.

Herein, graphene-carbon nanofiber paper (GCP) is prepared using graphite oxide (GO) and CNFs as the precursors, then the GCP is used as substrate for depositing MnO_2 nanosheets. Compared to other freestanding electrode materials, the GCP can be facile and scalable synthesized. After dipping

in KMnO_4 solution for a certain time, the surface of GCP would be uniformly covered by a layer of MnO_2 nanosheets. As no any additional binders or conductive additives are used in the preparation of electrodes, these MnO_2 -deposited composite papers exhibit an excellent capacitive performance with 298.2 F g^{-1} at 1 A g^{-1} , outstanding rate capability, and high stability. Hence, this work would be beneficial to develop high electrochemical performance, flexible, and binder-free electrode materials for supercapacitors.

Experimental

Materials preparation

Reagents used in this experiment, such as potassium permanganate (KMnO_4), sulfuric acid (H_2SO_4), nitric acid (HNO_3), and ethyl alcohol, were of analytical grade without further purification. CNFs, synthesized by a vapor-grown method, was purchased from Shenzhen Dynanonic (China) and sodium L-ascorbate was purchased from Sigma-Aldrich.

Synthesis of graphene-carbon nanofiber paper (GCP)

Graphite oxide (GO) was synthesized from graphite powder (Sigma-Aldrich) according to a modified Hummer's method [41]. CNFs were acidified by a mixed acid ($V_{(\text{HNO}_3)}/V_{(\text{H}_2\text{SO}_4)}=3:1$) at $90 \text{ }^\circ\text{C}$ for 2 h to increase the dispersity of CNFs in water as well as remove the impurities. GCP was prepared by the following procedures. In detail, a certain amount of CNFs were dispersed in 1 mL of 2 mg mL^{-1} GO suspension by ultrasonication to get a homogeneous GO-CNFs solution. The weight ratio of CNFs/GO can be changed in the experiment, which was 1:1 in this study, then uniformly covering the result solution onto a $6 \text{ cm} \times 8 \text{ cm}$ Al foil and removing most of the water by drying at $80 \text{ }^\circ\text{C}$ for 3 h. After cutting the Al foil into round pieces with a diameter of 6 mm, the GO-CNFs pieces were obtained after dissolution of Al foil using 3 mol L^{-1} HCl. The reduction of GO was conducted by keeping GO-CNFs pieces in 3 mL of 2 mg mL^{-1} sodium L-ascorbate solution at $90 \text{ }^\circ\text{C}$ for 3 h, then the graphene-CNFs pieces were washed with absolute ethyl alcohol and deionized water several times. For ease of description, all these graphene-CNFs pieces were denoted as GCP. For comparison, the pure graphene paper was also prepared without addition of CNFs.

Synthesis of graphene-carbon nanofiber/ MnO_2 nanocomposite paper (GMP) and CNFs- MnO_2 composite (CM)

The growth of MnO_2 nanostructures was carried out by immersing the GCP piece into 2 mL acidic KMnO_4 solution at $70 \text{ }^\circ\text{C}$. The mass loading of MnO_2 can be strictly controlled by

changing the concentration of KMnO_4 , which was 0.005 mol L^{-1} in this study. The MnO_2 -deposited GCP piece was taken out when the purple color of KMnO_4 was faded. After being thoroughly rinsed with deionized water, the MnO_2 -deposited GCP was dried at 80°C for 12 h and denoted as GMP (the main preparation processes of GMP are also shown in Fig. 1). For highlighting the electrochemical performances of the binder-free GMP electrodes, the CNFs- MnO_2 composite (CM) was prepared by acidified CNFs and KMnO_4 . Here, we chose out the CM that has the best electrochemical performances. Detailedly, 50 mg acidified CNFs was uniformly dispersed in deionized water and 150 mg KMnO_4 was dissolved in under magnetic stirring. After addition of some 1 mol L^{-1} sulfuric acid, the as-prepared solution was kept at 70°C until the purple color of KMnO_4 faded into golden brown. Finally, the product was filtered out and rinsed with deionized water several times and dried at 80°C for 12 h. For comparison, the graphene/ MnO_2 composite paper was also prepared under the same conditions using pure graphene paper as the substrate.

Synthesis of 3D graphene-CNFs composite (GC)

To construct an asymmetric supercapacitor with GMP as the positive electrode, the negative electrode material (3D graphene-CNFs (GC)) was also prepared here with our method [42]. In detail, a appropriate amount of CNFs were dispersed in 1 mg mL^{-1} GO suspension by ultrasonication to get a homogeneous GO-CNFs solution, in which the weight ratio of GO/CNFs was 5:2 (the selection of mass ratio of GO/CNFs is based on our earlier reports [42] and the reference [43]). Then the result solution was loaded in a glass vial and 3-fold weight of GO of sodium L-ascorbate was added in. Finally, the glass vial was sealed and kept at 90°C for 3 h without any disturbance to produce GC. After washed with ethyl alcohol and deionized water, GC was freeze-dried for use.

Materials characterizations

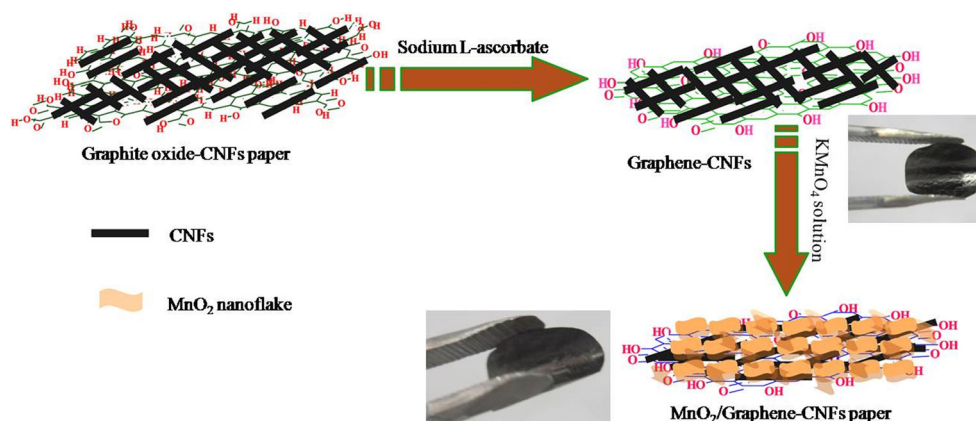
The phase identification of as-prepared samples were conducted by a MXPAHF X-ray diffractometer (Xpert, Philips) using a Cu $K\alpha$ radiation. Raman spectra were obtained using a LabRAM HR UV/vis/NIR spectrometer (Horiba Jobin Yvon, France) with an Ar ion CW laser (514.5 nm) as the excitation source. The microstructures of the samples were examined by a field-emission scanning electron microscope (FE-SEM, FEI Nova Nano-230). The energy dispersive spectroscopy (EDS, Bruker EDS Quantax 4010) was used to analyze the elements in the products. The surface chemistry of GMP was investigated by a PHI Quantera Imaging X-ray photoelectron spectroscopy (XPS). The mass of MnO_2 in GMP was obtained by the thermogravimetric analysis (TGA) which was carried out on a DTA-50 thermal analyzer (Shimadzu, Japan) in the temperature range of $30\text{--}800^\circ\text{C}$ with a heating rate of $5^\circ\text{C}/\text{min}$ in air atmosphere.

Electrochemical measurements

Fabrication of working electrodes

To evaluate the electrochemical performances of the products. The GCP and GMP were directly pressed on $1 \text{ cm} \times 1 \text{ cm}$ stainless foil at 15 MPa to use as the working electrode in the tests, while the CM electrode was made through a traditional method that we previously reported [4]. In brief, CM, carbon black, and polytetrafluoroethylene (PTFE, 10 wt%) were mixed in a weight ratio of 8:1:1 to get a mixture. The mixture was then rolled into a thin film. Finally, the film was pressed onto a $1 \text{ cm} \times 1 \text{ cm}$ stainless foil at 15 MPa and dried at 60°C for 12 h. The mass of active materials in all electrodes were about 1.2–1.6 mg. All electrochemical tests were carried out in 1 mol L^{-1} Na_2SO_4 solution by a three-electrode cell at ambient temperature. A platinum plate and a saturated calomel electrode (SCE) were used as the counter electrode and the

Fig. 1 Schematic illustration of the formation processes of the GMP



reference electrode of the cell, respectively. The electrochemical instrument was the CHI660B electrochemical workstation (Shanghai, China).

Fabrication of the asymmetric supercapacitor and data analysis of electrochemical measurements

To fabricate GMP//GC asymmetric supercapacitor, the mass ratio of the loaded active materials was estimated based on the calculated specific capacitances of GMP and GC from their discharge curves according to Eq. (2). The positive and negative electrodes of GMP//GC supercapacitor was separated with a glass-fiber separator before assembling into a two-electrode cell. The electrochemical properties of GMP//GC supercapacitor were also tested by cyclic voltammetry (CV) and galvanostatic charge/discharge techniques on the CHI660B electrochemical workstation. The specific capacitances of all electrodes and the asymmetric supercapacitor were calculated based on the CVs and discharge curves according to Eqs. (1) and (2), respectively. The energy density (E , Wh kg⁻¹) and power density (P , kW kg⁻¹) for asymmetric supercapacitors were calculated using the following Eqs. (3) and (4), respectively [34].

$$C = \frac{Q}{\Delta V} = \frac{1}{mv(V_a - V_c)} \int_{V_a}^{V_c} I(V) dV \quad (1)$$

$$C = \frac{I \times \Delta t}{\Delta V \times m} \quad (2)$$

$$E = 0.5C(\Delta V)^2/3.6 \quad (3)$$

$$P = E \ 3600/\Delta t \quad (4)$$

where m is the total mass of the active materials on both electrodes, v is the potential scan rate (mV s⁻¹), I is the

constant discharge current, Δt is the discharging time, and ΔV is the voltage drop upon discharging (excluding IR drop).

Results and discussion

Structures characterization

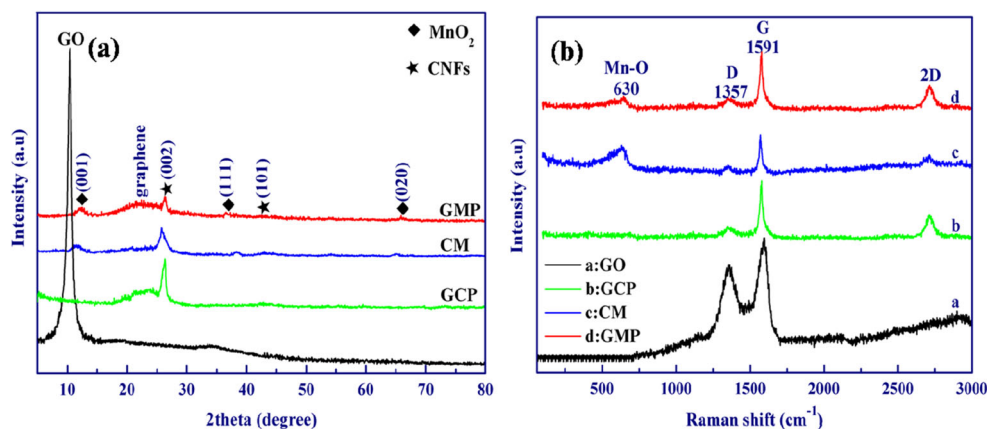
The in situ growth of MnO₂ nanostructures on GCP can be attributed to the redox reaction between KMnO₄ and carbon materials in acidic solution. The chemical reaction is formulated as follows [9].



X-ray diffraction (XRD) patterns of GO, GCP, CM, and GMP are shown in Fig. 2a. As observed, both patterns present the characteristic diffraction peaks of birnessite-type MnO₂ (δ -MnO₂) at 12°, 37°, and 66° (2θ) (JCPDS No. 42-1317) [44–46], while the other two peaks at 26° and 43° (2θ) are indexed to the characteristic peaks of CNFs [24, 45]. Different to CM, an additional peak at 24° (2θ) is observed for GMP because of the existence of graphene [24]. Note that the characteristic peak of GO, which usually appeared at 10.3° (2θ), is not found on the XRD pattern of GMP, indicating that GO has been successfully reduced to graphene in the preparation of GCP [47].

Raman spectra of GO, GCP, CM, and GMP are displayed in Fig. 2b. Both spectra show the D and G bands at 1357 and 1591 cm⁻¹, respectively. For higher intensity ratio of D-bond to G-bond (I_D/I_G) in GMP (0.27) comparing to that of CM (0.23), it can be assigned reasonably to the fact that some structural defects exist in graphene in GMP [48, 49]. The increased I_D/I_G ratio of graphene after chemical reduction has been commonly reported in the literature [50], while the I_D/I_G ratios of GMP is much lower than that of GO (0.8) here.

Fig. 2 XRD patterns (a) and Raman spectra (b) of GO, GCP, CM, and GMP



This can be attributed to the existence of CNFs in GMP. The CNFs, which were synthesized by a vapor-grown method, have few structural defects. The CNFs account for about 50.0 wt% in GCP; thus, the GMP would show a low level of defects in its structure. The more sharp 2D peaks at 2693 cm^{-1} in both GCP and GMP than that of CM indicates the existence of graphene in GC and GCM [51]. Additionally, the intense peak at 630 cm^{-1} on both spectra can be attributed to the symmetric Mn-O stretching vibration of the MnO_6 in MnO_2 , further indicating the formation of MnO_2 in GMP [52].

To better understand the chemical composition and the oxidation state of the Mn element in GMP, the XPS measurement was conducted as shown in Fig. 3a. The signals of Mn, O, K, and C elements can be observed on the spectrum. For the presence of K element in the spectrum, it can be attributed to the hydrated K^+ cations in the interlayer of $\delta\text{-MnO}_2$. In the C1s peak (Fig. 3b), the oxygen-containing functional groups present only smaller intensities indicates that the GO is well reduced by sodium L-ascorbate. The peaks at 284.5, 285.7, 286.6, and 288.3 eV can be owned to the non-oxygenated carbon, carbon in C-O (hydroxyl and epoxy groups), C=O (carbonyl groups), and O-C=O (carboxyl groups), respectively [4]. In Mn 2p spectrum (Fig. 3c), the characteristic binding energies of Mn $2p_{1/2}$ and Mn $2p_{3/2}$ peaks can be detected at 654.1 and 642.3 eV, respectively. As no peak at 647 eV is found on the spectrum and the binding energies separation of Mn 2p is 11.8 eV, indicating that MnO_2 was successfully

grown on GCP [8, 36, 45]. Additionally, the Mn 3s spectrum is shown in Fig. 3d to further determine the oxidation state of Mn. The peak splitting width (ΔE) of the Mn 3s doublet is 4.94 eV and the average valence of Mn in GMP is calculated to be 3.7 according to the method reported previously [7].

Morphologies characterization

Figure 4 presents the SEM images of graphene paper (GP) (Fig. 4a–c) and GCP (Fig. 4d–h). GP shows a quite smooth surface with tightly stacked graphene nanosheets. After incorporation of CNFs, the GCP displays a highly wrinkled surface (Fig. 4d–f) which would be beneficial to the growth of MnO_2 nanostructures. In addition, the existence of CNFs in GCP greatly prevent the aggregation of graphene nanosheets, then resulting in a much wider interlayer spacing (about $2\text{ }\mu\text{m}$, Fig. 4g–i) compared to that of GP. Figure 5 shows the SEM images of CM and GMP. In the low- (Fig. 5a) and high magnification (the inset of Fig. 5a) SEM images of CM, we can see that MnO_2 nanoflakes were uniformly grown on the surface of CNFs without bulk agglomeration, while these MnO_2 -deposited carbon nanofibers agglomerate each other. In contrast, the thinner MnO_2 nanoflakes are observed to be uniformly grown on GCP (Fig. 5b, c) with the walls of MnO_2 nanoflake interconnected each other. In Fig. 5d, the EDX spectroscopy of GMP further indicates the existence of C, O, and Mn elements, while the signal of K element can be attributed to K^+ ion in birnessite-type MnO_2 well

Fig. 3 XPS spectra of **a** survey scan; **b** C1s region; **c** Mn 2p region; and **d** Mn 3s region of GMP

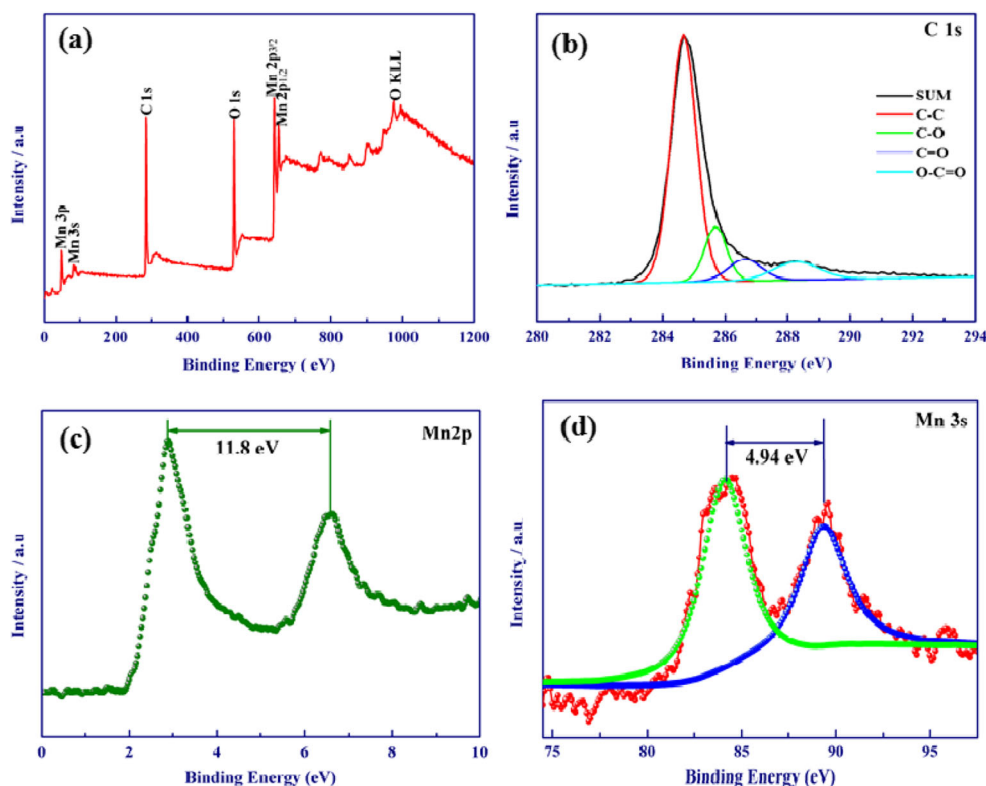
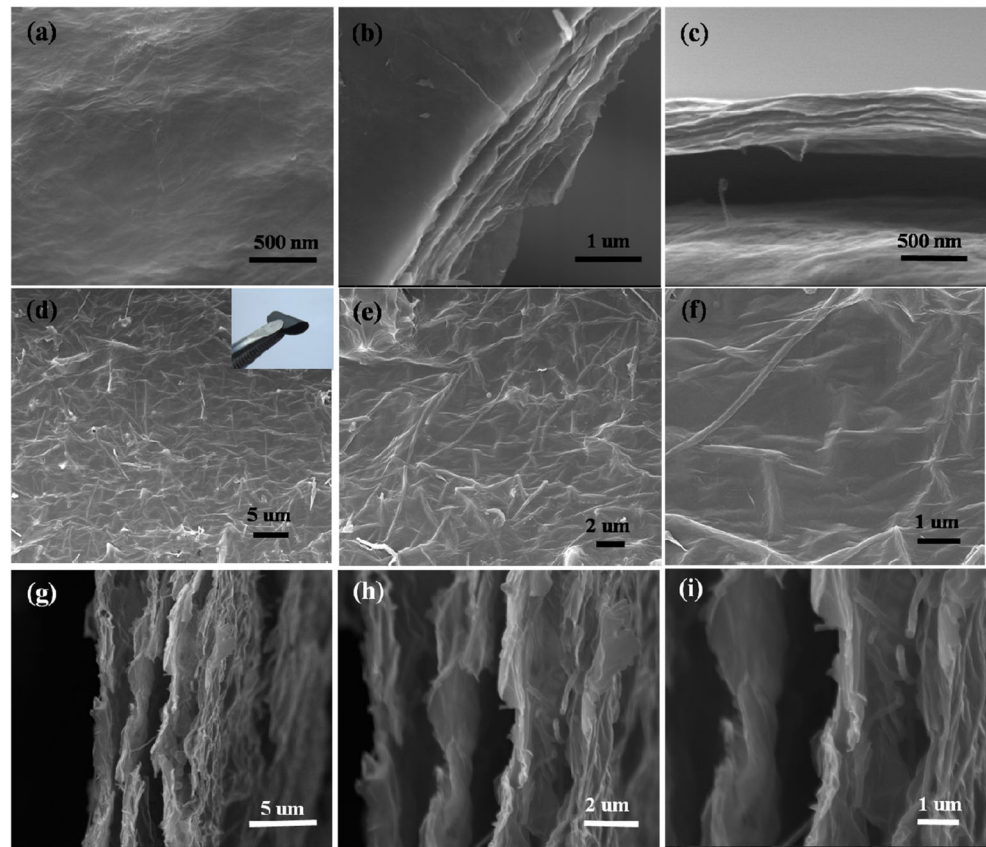


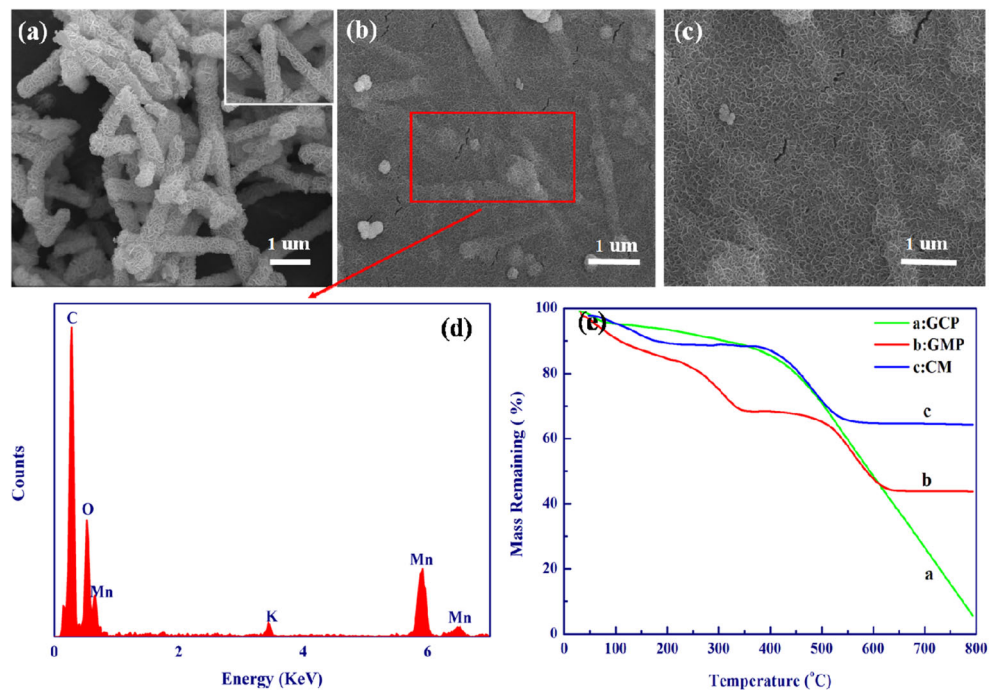
Fig. 4 Low- and high-magnification SEM images of GP (a–c); low- and high-magnification SEM images of GCP (d–f); cross-section SEM images of GCP (g–i)



consistent with the result of XPS spectrum [3]. Furthermore, the MnO_2 content in GMP has been investigated by the TGA. As seen from the TGA spectra of GCP, GMP, and CM (Fig. 5e), there are two steps for

mass loss with the temperature increasing. The mass loss before 300 °C can be ascribed to the removal of absorbed water in the hybrids, while the removal of carbon atom in GMP composites can be detected to

Fig. 5 SEM images of GMP (a); low- and high-magnification SEM images of GMP (b, c); EDX spectroscopy of the selected area of GMP (d); the thermal gravimetric analysis (TGA) spectra of GCP, CM, and GMP



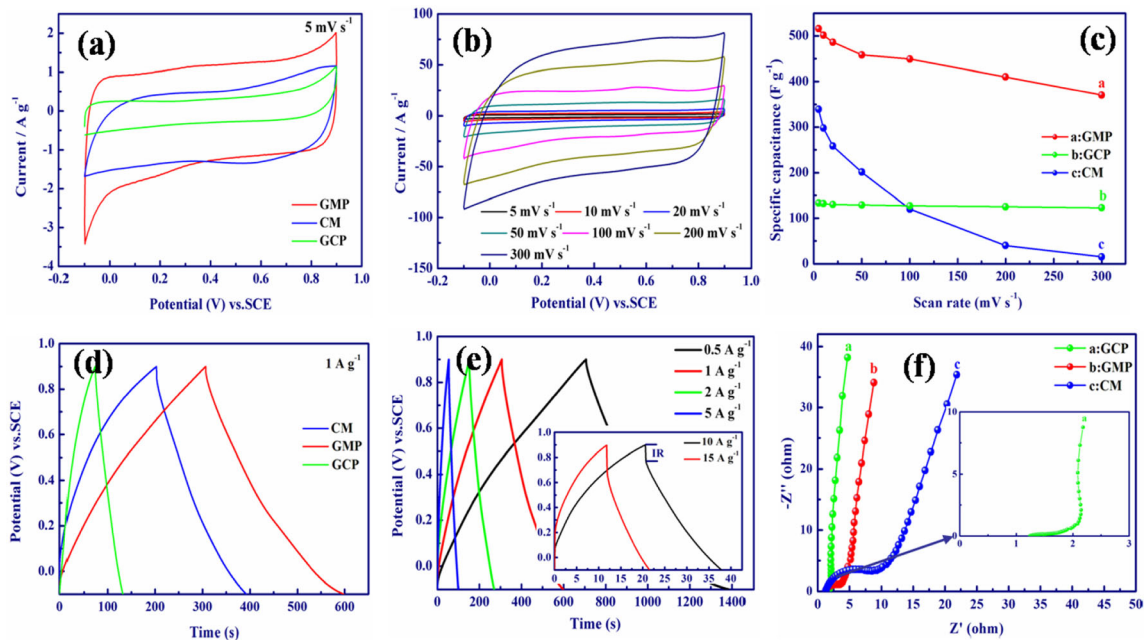


Fig. 6 a CVs of GCP, CM, and GMP at 5 mV s^{-1} ; b CVs of GMP at various scan rates from 5 to 300 mV s^{-1} ; c a comparison of specific capacitance of GCP, CM, and GMP electrodes at different scan rates; d galvanostatic discharge curves of GCP, CM, and GMP electrodes at

1.0 A g^{-1} ; e galvanostatic charge–discharge curves of GMP at different current densities (0.5 to 15 A g^{-1}); f Nyquist plots for GCP, CM, and GMP electrodes

the mass loss at $500\text{--}600 \text{ }^\circ\text{C}$ [4]. Therefore, the mass ratio of MnO_2 in hybrids is demonstrated to be 42.5 wt%.

Electrochemical performances of GMP

Figure 6a shows the cyclic voltammetry curves (CVs) of GCP, CM and GMP electrodes in $1 \text{ M Na}_2\text{SO}_4$ at a scan rate of 5 mV/s . The potential window for cycling is confined between -0.1 and 0.9 V versus SCE to avoid the oxygen evolution

reaction at higher potentials and manganese dissolution at lower potentials [9, 53, 54]. Three CVs display a rectangular-like shape and the GMP electrode has the largest CV curve area, indicating the best capacitive performance of GMP electrode [9]. Gravimetric current of GMP is much higher than GCP and CM electrodes due to the existence of pseudocapacitive MnO_2 and freestanding structure, which results in higher gravimetric capacitance. The rate-dependent CVs of GMP electrode was investigated at various scan rates from 5 to 300 mV s^{-1} , as shown in Fig. 6b. The rate capability

Table 1 Comparison of capacitive performance of supercapacitors based on various binder-free MnO_2 /carbon composites presented in literatures and the present work

Samples	C	Electrolyte	E	T	$C_7\%$	Ref
MnO_2 -CNT-textile	410.0 (5 mV s^{-1})	$0.5 \text{ M Na}_2\text{SO}_4$	17.5 (10)	10,000	60.0 %	[8]
Whisker-like MnO_2 /carbon fiber paper	274.1 (0.1 A g^{-1})	$1.0 \text{ M Na}_2\text{SO}_4$	–	5000	95.0 %	[28]
MnO_2 -graphene on carbon fiber paper	393.0 (0.1 A g^{-1})	$0.5 \text{ M Na}_2\text{SO}_4$	–	2000	98.5 %	[55]
MnO_2 /CNT/papers	540.0 (2 mV s^{-1})	$0.1 \text{ M Na}_2\text{SO}_4$	20.5 (1.5)	1000	95.0 %	[56]
Graphene/ MnO_2 papers	256.0 (0.5 A g^{-1})	$0.1 \text{ M Na}_2\text{SO}_4$	–	1000	74.0 %	[57]
Graphene/ MnO_2 paper	217.0 (0.1 A g^{-1})	$1.0 \text{ M Na}_2\text{SO}_4$	–	3600	93.0 %	[58]
Graphene-patched CNT/ MnO_2 papers	225.0 (1.0 A g^{-1})	$1.0 \text{ M Na}_2\text{SO}_4$	24.8 (0.2)	800	92.8 %	[59]
MnO_2 nanowires/CNT paper	167.5 (0.077 A g^{-1})	$0.1 \text{ M Na}_2\text{SO}_4$	–	3000	88.0 %	[60]
MnO_2 nanoflakes/carbon paper	306.5 (0.5 A g^{-1})	$1.0 \text{ M Na}_2\text{SO}_4$	20.8 (0.09)	6000	97.1 %	[18]
MnO_2 nanoflakes/graphene-CNF paper	298.2 (1 A g^{-1}) 515.5 (5 mV s^{-1})	$1.0 \text{ M Na}_2\text{SO}_4$	23.0 (0.45)	3000	95.7 %	This work

C the specific capacitance (F g^{-1}), calculated based on the scan rate (mV s^{-1}) or the current density (A g^{-1}) in a three-electrode system, E the energy density (Wh kg^{-1}) based on the power density (kW kg^{-1}) in a supercapacitor, T cycles of cycle life test, $C_7\%$ retention rate of specific capacitance after cycle life test

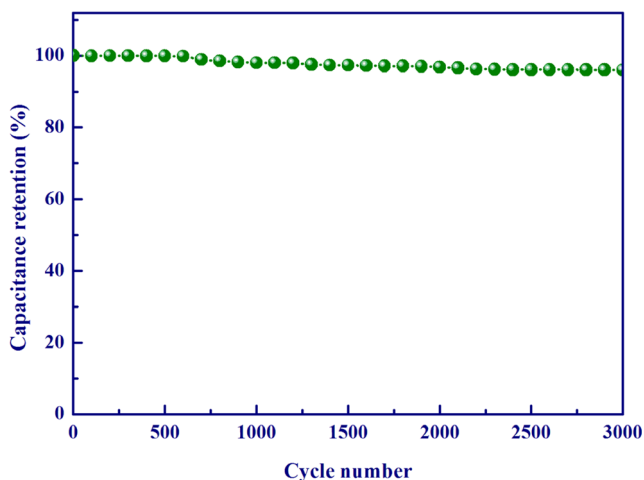


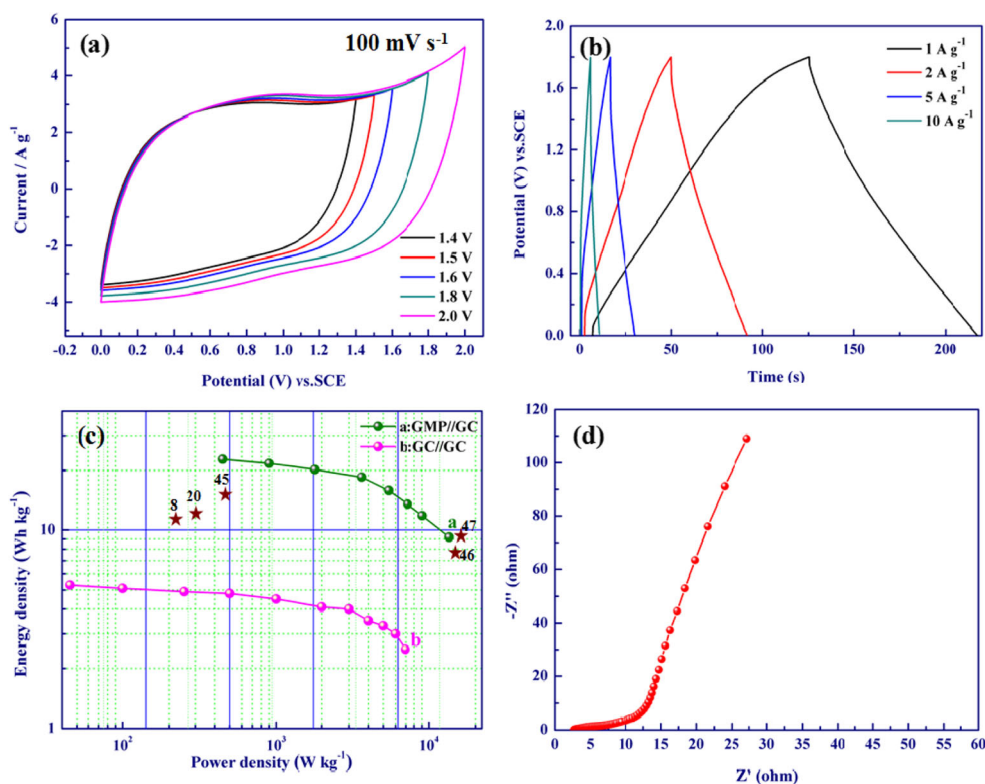
Fig. 7 Cycling performances of GMP electrode at 5.0 A g^{-1}

of GMP electrode is excellent, and it maintains a good rectangular CV shape with only small distortions even at 300 mV s^{-1} , which results in only $\sim 28.2\%$ loss of capacitance compared to those measured at 5 mV s^{-1} (Fig. 6c). In contrast to previous work, this result also shows a good improvement in the rate capability, which is summarized in Table 1. As for the 92.5% of capacitance retention of GCP electrode, it suggests that GCP has not only good electronic conductivity but also could offer a certain amount of double electric layer capacitance (DEL). For $\sim 95.6\%$ loss of capacitance in CM electrode, it can be attributed to the addition of binders in the electrode preparation, which greatly increases its inner

resistance. Furthermore, the high gravimetric capacitances of GMP electrode at high scan rates are superior or comparable to those of previous studies (Table 1).

Galvanostatic charge/discharge curves of GMP, CM, and GCP electrodes at a current density of 1 A g^{-1} are shown in Fig. 6d; three curves present a typical triangular-shape with good symmetry and fairly linear slope, indicating the good capacitive characteristic of these electrodes. The specific capacitance of GMP electrode is calculated to be 298.2 F g^{-1} (1 A g^{-1}) based on the discharge curve via Eq. (2), which is much higher than that of GCP and CM electrodes. The rate-dependent galvanostatic charge/discharge curves of GMP electrode was investigated at various current densities from 0.5 to 15 A g^{-1} , as shown in Fig. 6e. The excellent rate capability of GMP electrode is further demonstrated as the voltage (IR) drop on curves can be negligible until the high current density of 10 A g^{-1} . Electrochemical impedance spectroscopy measurements were performed under open circuit potential in an alternating current frequency range of 0.01 to $100,000 \text{ Hz}$ with an excitation signal of 5 mV . The electrochemical impedance spectra (EIS) acquired are shown as the Nyquist plots in Fig. 5f, all which exhibit a typical arc at the high-frequency region and a spike at the low-frequency region [61]. The diameter of semicircle presents the charge-transfer resistance (R_{ct}) in the electrochemical system. The R_{ct} of the GCP electrode is only $\sim 1.1 \Omega$, indicating that it is an excellent substrate with high electronic conductivity for depositing nanosized MnO_2 . Meanwhile, the R_{ct} values of the GMP

Fig. 8 **a** CVs of an optimized GMP//GC asymmetric supercapacitor measured in a potential window from 1.4 to 2.0 V at 100 mV s^{-1} ; **b** galvanostatic charge/discharge curves of GMP//GC asymmetric cell at 1.0 – 10 A g^{-1} ; **c** Ragone plots of the GMP//GC and GC//GC supercapacitors; **d** EIS spectrum of the GMP//GC asymmetric supercapacitor



and CM electrodes are ~ 2.1 and $\sim 8.8 \Omega$, respectively, suggesting that no addition of any binders in GMP electrode allows it to have good electronic conductivity.

The cycling stability of the GMP electrode is carried out by repeating the galvanostatic charge–discharge test within -0.1 to 0.9 V at a current density of 5 A g^{-1} (Fig. 7). The GMP electrode exhibits an excellent electrochemical stability with only 4.3 % deterioration of its initial specific capacitance after 3000 cycles. Generally, the capacitance loss is attributed to the factors such as the dissolution of MnO_2 in the electrolyte, mechanical faults of the electrodes (e.g., expansion, agglomeration and detachment of MnO_2 , corrosion of the current collectors) and the instability of the electrode potential caused by imbalanced capacity on two electrodes [62]. Here, we ascribe the long-term cycling stability of GMP electrode to the good attachment between MnO_2 and GCP substrate, and the microstructure of MnO_2 .

Finally, to investigate the practical performance of the GMP electrode, we assembled a GMP//GC asymmetric supercapacitor (the detailed fabrication method is shown in the experimental portion). Figure 8a presents the CV curves of the asymmetric supercapacitor at various potential windows with a scan rate of 100 mV s^{-1} . It is found that the CVs keep well of a rectangular-like shape until 2.0 V, indicating that the GMP//GC asymmetric supercapacitor has good capacitive performance and can be operated at high voltage. Its corresponding charge/discharge curves at different current densities are shown in Fig. 8b. The supercapacitor shows a stable Coulombic efficiency (CE) near 90 %. Its CE is kept at 85.7 % even at the high current of 10 A g^{-1} . Figure 8c shows the Ragone plot of the energy density versus power density considering the total mass of active materials from positive and negative electrodes. According to the Eqs. 2, 3, and 4, the supercapacitor exhibits a maximum energy density of 23.0 Wh kg^{-1} at 450.8 W kg^{-1} , in which the operating voltage is 1.8 V. Compared to similar systems reported previously using symmetric MnO_2 // MnO_2 [63], or other hybrid MnO_2 //carbon-based materials (CNTs or active carbon) [34, 54, 64–66] or MnO_2 //PEDOT [67], this asymmetric supercapacitor exhibits comparable energy density. Nyquist plot of the asymmetric supercapacitor over the frequency range of 0.01–100,000 Hz is presented in Fig. 8d. Its R_{ct} is about 8.2Ω , further indicating that this asymmetric supercapacitor has a low internal resistance for high-rate power delivery.

Conclusions

In summary, we have successfully prepared flexible and free-standing graphene-carbon nanofiber/ MnO_2 nanocomposite paper (GMP) via a simple method. The MnO_2 nanoflakes are uniformly deposited on the surface of paper and exhibit a porous structure by interconnecting each other. The capacitive

performance of the GMP electrode was studied by electrochemical techniques. We found that the as-prepared composite paper showed high specific capacitance, excellent rate capability, and good stability due to its binder-free porous structure and the wrinkled structure of MnO_2 nanoflakes. In a practical application test, the GMP-based asymmetric supercapacitor also exhibits an excellent electrochemical performance with a high operating voltage of 2.0 V and a high energy density of 23.0 Wh kg^{-1} at 450.8 W kg^{-1} . We believe that the composite paper would be potentially promising as electrode materials for flexible and high performance supercapacitors.

Acknowledgments The authors acknowledge the funds from the Chinese National Natural Science Foundation (Nos.51372278).

References

1. Simon P, Gogotsi Y (2008) Materials for electrochemical capacitors. *Nat Mater* 7:845–854
2. Zhu Y, Murali S, Stoller MD, Ganesh KJ, Cai W, Ferreira PJ, Pirkle A, Wallace RM, Cychosz KA, Thommes M, Su D, Stach EA, Ruoff RS (2011) Carbon-based supercapacitors produced by activation of graphene. *Science* 332:1537–1541
3. Wang J-G, Yang Y, Huang Z-H, Kang F (2012) Synthesis and electrochemical performance of MnO_2 /CNTs-embedded carbon nanofibers nanocomposites for supercapacitors. *Electrochim Acta* 75:213–219
4. Wu Y, Liu S, Wang H, Wang X, Zhang X, Jin G (2013) A novel solvothermal synthesis of Mn_3O_4 /graphene composites for supercapacitors. *Electrochim Acta* 90:210–218
5. Yan J, Fan Z, Wei T, Qian W, Zhang M, Wei F (2010) Fast and reversible surface redox reaction of graphene– MnO_2 composites as supercapacitor electrodes. *Carbon* 48:3825–3833
6. Cheng Q, Tang J, Ma J, Zhang H, Shinya N, Qin L-C (2011) Graphene and nanostructured MnO_2 composite electrodes for supercapacitors. *Carbon* 49:2917–2925
7. Wang J-G, Yang Y, Huang Z-H, Kang F (2013) A high-performance asymmetric supercapacitor based on carbon and carbon– MnO_2 nanofiber electrodes. *Carbon* 61:190–199
8. Hu L, Chen W, Xie X, Liu N, Yang Y, Wu H, Yao Y, Pasta M, Alshareef HN, Cui Y (2011) Symmetrical MnO_2 –carbon nanotube–textile nanostructures for wearable pseudocapacitors with high mass loading. *ACS Nano* 5:8904–8913
9. Lee SW, Kim J, Chen S, Hammond PT, Shao-Horn Y (2010) Carbon nanotube/manganese oxide ultrathin film electrodes for electrochemical capacitors. *ACS Nano* 4:3889–3896
10. Jaidev RI, Jafri AK, Mishra S (2011) Ramaprabhu, polyaniline– MnO_2 nanotube hybrid nanocomposite as supercapacitor electrode material in acidic electrolyte. *J Mater Chem* 21:17601
11. Jiang H, Ma J, Li C (2012) Polyaniline– MnO_2 coaxial nanofiber with hierarchical structure for high-performance supercapacitors. *J Mater Chem* 22:16939
12. Huang L, Chen D, Ding Y, Feng S, Wang ZL, Liu M (2013) Nickel–cobalt hydroxide nanosheets coated on NiCo_2O_4 nanowires grown on carbon fiber paper for high-performance pseudocapacitors. *Nano Lett* 13:3135–3139
13. Hao Q, Wang J, Xu C (2014) Facile preparation of Mn_3O_4 octahedra and their long-term cycle life as an anode material for Li-ion batteries. *J Mater Chem A* 2:87–93

14. Perera SD, Patel B, Nijem N, Roodenko K, Seitz O, Ferraris JP, Chabal YJ, Balkus KJ (2011) Vanadium oxide nanowire-carbon nanotube binder-free flexible electrodes for supercapacitors. *Adv Energy Mater* 1:936–945
15. Wang G, Zhang L, Zhang J (2012) A review of electrode materials for electrochemical supercapacitors. *Chem Soc Rev* 41:797–828
16. Xia C, Ning W, Lin G (2009) Facile synthesis of novel MnO₂ hierarchical nanostructures and their application to nitrite sensing. *Sensors Actuators B Chem* 137:710–714
17. Li X, Wei B (2012) Facile synthesis and super capacitive behavior of SWNT/MnO₂ hybrid films. *Nano Energy* 1:479–487
18. He S, Hu C, Hou H, Chen W (2014) Ultrathin MnO₂ nanosheets supported on cellulose based carbon papers for high-power supercapacitors. *J Power Sources* 246:754–761
19. Cao F, Liu Y, Chen B, Fei L, Wang Y, Yuan J (2012) Enhancement of electrochemical capacitive properties based on complementation of morphologies. *Electrochim Acta* 81:1–7
20. Wang Y-T, Lu A-H, Zhang H-L, Li W-C (2011) Synthesis of nanostructured mesoporous manganese oxides with three-dimensional frameworks and their application in supercapacitors. *J Phys Chem C* 115:5413–5421
21. Ni J, Lu W, Zhang L, Yue B, Shang X, Lv Y (2008) Low-temperature synthesis of monodisperse 3D manganese oxide nanoflowers and their pseudocapacitance properties. *J Phys Chem C* 113:54–60
22. Zhai D, Li B, Du H, Gao G, Gan L, He Y, Yang Q, Kang F (2012) The preparation of graphene decorated with manganese dioxide nanoparticles by electrostatic adsorption for use in supercapacitors. *Carbon* 50:5034–5043
23. Wang Y, Yu SF, Sun CY, Zhu TJ, Yang HY (2012) MnO₂/onion-like carbon nanocomposites for pseudocapacitors. *J Mater Chem* 22:17584–17588
24. Zhao X, Zhang L, Murali S, Stoller MD, Zhang Q, Zhu Y, Ruoff RS (2012) Incorporation of manganese dioxide within ultraporous activated graphene for high-performance electrochemical capacitors. *ACS Nano* 6:5404–5412
25. Hassab S, Padilla J (2014) Use of ionic liquids in electrochromic devices. *Ionic Liquids in Separation Technology* 301
26. Choi BG, Huh YS, Hong WH, Kim HJ, Park HS (2012) Electrochemical assembly of MnO₂ on ionic liquid–graphene films into a hierarchical structure for high rate capability and long cycle stability of pseudocapacitors. *Nanoscale* 4:5394–5400
27. Pushparaj VL, Shaijumon MM, Kumar A, Murugesan S, Ci L, Vajtai R, Linhardt RJ, Nalamasu O, Ajayan PM (2007) Flexible energy storage devices based on nanocomposite paper. *Proc Natl Acad Sci* 104:13574–13577
28. Luo Y, Jiang J, Zhou W, Yang H, Luo J, Qi X, Zhang H, Yu DYW, Li CM, Yu T (2012) Self-assembly of well-ordered whisker-like manganese oxide arrays on carbon fiber paper and its application as electrode material for supercapacitors. *J Mater Chem* 22:8634
29. Gao H, Xiao F, Ching CB, Duan H (2012) Flexible all-solid-state asymmetric supercapacitors based on free-standing carbon nanotube/graphene and Mn₃O₄ nanoparticle/graphene paper electrodes. *ACS Appl Mater Interfaces* 4:7020–7026
30. Yang L, Cheng S, Ding Y, Zhu X, Wang ZL, Liu M (2012) Hierarchical network architectures of carbon fiber paper supported cobalt oxide nanonet for high-capacity pseudocapacitors. *Nano Lett* 12:321–325
31. Huang X, Qi X, Boey F, Zhang H (2012) Graphene-based composites. *Chem Soc Rev* 41:666–686
32. Butler SZ, Hollen SM, Cao L, Cui Y, Gupta JA, Gutierrez HR, Heinz TF, Hong SS, Huang J, Ismach AF (2013) Progress, challenges, and opportunities in two-dimensional materials beyond graphene. *ACS Nano* 7:2898–2926
33. Zhu J, Yang D, Yin Z, Yan Q, Zhang H (2014) Graphene and graphene-based materials for energy storage applications. *Small* 10:3480–3498
34. Gao H, Xiao F, Ching CB, Duan H (2012) High-performance asymmetric supercapacitor based on graphene hydrogel and nanostructured MnO₂. *ACS Appl Mater Interfaces* 4:2801–2810
35. Ra EJ, Raymundo-Piñero E, Lee YH, Béguin F (2009) High power supercapacitors using polyacrylonitrile-based carbon nanofiber paper. *Carbon* 47:2984–2992
36. Kim C (2005) Electrochemical characterization of electrospun activated carbon nanofibres as an electrode in supercapacitors. *J Power Sources* 142:382–388
37. Koziol K, Vilatela J, Moissala A, Motta M, Cunniff P, Sennett M, Windle A (2007) High-performance carbon nanotube fiber. *Science* 318:1892–1895
38. Lu X, Zhai T, Zhang X, Shen Y, Yuan L, Hu B, Gong L, Chen J, Gao Y, Zhou J (2012) WO₃-x@ Au@ MnO₂ core-shell nanowires on carbon fabric for high-performance flexible supercapacitors. *Adv Mater* 24:938–944
39. Cheng Q, Tang J, Ma J, Zhang H, Shinya N, Qin L-C (2011) Polyaniline-coated electro-etched carbon fiber cloth electrodes for supercapacitors. *J Phys Chem C* 115:23584–23590
40. Hu L, Pasta M, Mantia FL, Cui L, Jeong S, Deshazer HD, Choi JW, Han SM, Cui Y (2010) Stretchable, porous, and conductive energy textiles. *Nano Lett* 10:708–714
41. Hummers WS, Offeman RE (1958) Preparation of graphitic oxide. *J Am Chem Soc* 80:1339–1339
42. Wu Y, Liu S, Zhao K, Yuan H, Lv K, Ye G (2015) Facile synthesis of 3D graphene hydrogel/carbon nanofibers composites for supercapacitor electrode. *ECS Solid State Letters* 4:M23–M25
43. Li X, Li T, Zhang X, Zhong Q, Li H, Huang J (2014) Chemical splitting of multiwalled carbon nanotubes to enhance electrochemical capacitance for supercapacitors. *Functional Materials Letters* 7: 1450057
44. Jiang H, Li C, Sun T, Ma J (2012) A green and high energy density asymmetric supercapacitor based on ultrathin MnO₂ nanostructures and functional mesoporous carbon nanotube electrodes. *Nanoscale* 4:807–812
45. Xia H, Lai M, Lu L (2010) Nanoflaky MnO₂/carbon nanotube nanocomposites as anode materials for lithium-ion batteries. *J Mater Chem* 20:6896–6902
46. Wang J-G, Yang Y, Huang Z-H, Kang F (2013) Effect of temperature on the pseudo-capacitive behavior of freestanding MnO₂@carbon nanofibers composites electrodes in mild electrolyte. *J Power Sources* 224:86–92
47. Xu Y, Sheng K, Li C, Shi G (2010) Self-assembled graphene hydrogel via a one-step hydrothermal process. *ACS Nano* 4:4324–4330
48. Moon IK, Lee J, Ruoff RS, Lee H (2010) Reduced graphene oxide by chemical graphitization. *Nat Commun* 1:1–6
49. Pei S, Zhao J, Du J, Ren W, Cheng H-M (2010) Direct reduction of graphene oxide films into highly conductive and flexible graphene films by hydrohalic acids. *Carbon* 48:4466–4474
50. Stankovich S, Dikin DA, Piner RD, Kohlhaas KA, Kleinhammes A, Jia Y, Wu Y, Nguyen ST, Ruoff RS (2007) Synthesis of graphene-based nanosheets via chemical reduction of exfoliated graphite oxide. *Carbon* 45:1558–1565
51. Some S, Kim Y, Yoon Y, Yoo H, Lee S, Park Y, Lee H (2013) High-quality reduced graphene oxide by a dual-function chemical reduction and healing process. *Sci Rep* 3
52. Lee S-W, Bak S-M, Lee C-W, Jaye C, Fischer DA, Kim B-K, Yang X-Q, Nam K-W, Kim K-B (2014) Structural changes in reduced graphene oxide upon MnO₂ deposition by the redox reaction between carbon and permanganate ions. *J Phys Chem C* 118:2834–2843

53. Brousse T, Taberna P-L, Crosnier O, Dugas R, Guillemet P, Scudeller Y, Zhou Y, Favier F, Bélanger D, Simon P (2007) Long-term cycling behavior of asymmetric activated carbon/MnO₂ aqueous electrochemical supercapacitor. *J Power Sources* 173:633–641
54. Brousse T, Toupin M, Belanger D (2004) A hybrid activated carbon-manganese dioxide capacitor using a mild aqueous electrolyte. *J Electrochem Soc* 151:A614–A622
55. Sawangphruk M, Srimuk P, Chiochan P, Krittayavathananon A, Luanwuthi S, Limtrakul J (2013) High-performance supercapacitor of manganese oxide/reduced graphene oxide nanocomposite coated on flexible carbon fiber paper. *Carbon* 60:109–116
56. Kang YJ, Kim B, Chung H, Kim W (2010) Fabrication and characterization of flexible and high capacitance supercapacitors based on MnO₂/CNT/papers. *Synth Met* 160:2510–2514
57. Li Z, Mi Y, Liu X, Liu S, Yang S, Wang J (2011) Flexible graphene/MnO₂ composite papers for supercapacitor electrodes. *J Mater Chem* 21:14706–14711
58. Sumboja A, Foo CY, Wang X, Lee PS (2013) Large areal mass, flexible and free-standing reduced graphene oxide/manganese dioxide paper for asymmetric supercapacitor device. *Adv Mater* 25:2809–2815
59. Jin Y, Chen H, Chen M, Liu N, Li Q (2013) Graphene-patched CNT/MnO₂ nanocomposite papers for the electrode of high-performance flexible asymmetric supercapacitors. *ACS Appl Mater Interfaces* 5:3408–3416
60. Chou S-L, Wang J-Z, Chew S-Y, Liu H-K, Dou S-X (2008) Electrodeposition of MnO₂ nanowires on carbon nanotube paper as free-standing, flexible electrode for supercapacitors. *Electrochem Commun* 10:1724–1727
61. Cheng Y, Lu S, Zhang H, Varanasi CV, Liu J (2012) Synergistic effects from graphene and carbon nanotubes enable flexible and robust electrodes for high-performance supercapacitors. *Nano Lett* 12:4206–4211
62. Yu G, Hu L, Liu N, Wang H, Vosgueritchian M, Yang Y, Cui Y, Bao Z (2011) Enhancing the supercapacitor performance of graphene/MnO₂ nanostructured electrodes by conductive wrapping. *Nano Lett* 11:4438–4442
63. Cottineau T, Toupin M, Delahaye T, Brousse T, Belanger D (2006) Nanostructured transition metal oxides for aqueous hybrid electrochemical supercapacitors. *Appl Phys A* 82:599–606
64. Fan Z, Yan J, Wei T, Zhi L, Ning G, Li T, Wei F (2011) Asymmetric supercapacitors based on graphene/MnO₂ and activated carbon nanofiber electrodes with high power and energy density. *Adv Funct Mater* 21:2366–2375
65. Wu Z-S, Ren W, Wang D-W, Li F, Liu B, Cheng H-M (2010) High-energy MnO₂ nanowire/graphene and graphene asymmetric electrochemical capacitors. *ACS Nano* 4:5835–5842
66. Khomenko V, Raymundo-Pinero E, Béguin F (2006) Optimisation of an asymmetric manganese oxide/activated carbon capacitor working at 2V in aqueous medium. *J Power Sources* 153:183–190
67. Khomenko V, Raymundo-Pinero E, Frackowiak E, Béguin F (2006) High-voltage asymmetric supercapacitors operating in aqueous electrolyte. *Appl Phys A* 82:567–573